Int. J. of Thermal & Environmental Engineering
Volume 1, No. 2 (2010) 91-98

Investigation on the Effect of Operating Parameters on the Performance of Solar Desiccant Cooling System Using Artificial Neural Networks

El-Shafei B. Zeidan*, Ayman A. Aly, Ahmed M. Hamed

Department of Mechanical engineering, Faculty of Engineering, Taif University, Al-Hawyah, PO Box 888, Saudi Arabia

Abstract

A multiple-layer artificial neural network (ANN) model has been applied to study the performance of a solar liquid-desiccant dehumidification/regeneration system. The experimental results of a previous study are used to construct and test the ANN model. Then the model has been utilized to describe the effect of the inlet conditions of the air and calcium chloride ($CaCl_2$) solution on the regeneration process. Good agreement between the outputs from the ANN model and the corresponding results from the experimental data has been found. The proposed model can work well as a predictive tool to complement the experiments.

Keywords: *Solar energy, dehumidification/regeneration, absorption, liquid desiccant, ANN, back propagation algorithm*

1. Introduction

Interest in utilizing solar-cooling systems for air-conditioning and refrigeration purposes has been growing continuously. Being considered as one path towards more sustainable energy systems, solar-cooling is comprised of many attractive features. This technology can efficiently serve large latent loads and greatly improve indoor air quality by allowing more ventilation while tightly controlling humidity [1]. On the other hand, solar-powered air conditioning has seen renewed interest in recent years due to the growing awareness of environmental problems such as global warming [2,3]. Solar collector/regenerator systems can achieve liquid regeneration at lower temperatures which is suitable for buildings with high outdoor air requirements in high humidity areas [4,5].

Several solar-driven refrigeration systems have been proposed and most of them are economically justified. These systems include sorption systems containing liquid/vapor or solid/vapor absorption/adsorption, vapor compression systems, and hybrid desiccant vapor compression systems [6]. The regenerator is one of the key components in liquid desiccant air-conditioning systems, in which desiccant is concentrated and can be reused in the system. The heat required for regenerating the weak desiccant solution is supplied into the regenerator by either hot air or hot desiccant solution. This heat can be provided by any form of low-grade thermal energy which is suitable for solar thermal applications. Different regenerator designs have been examined and a variety of theoretical models have been employed to analyze the regeneration process [7-12].

Theoretical models for solar desiccant cooling systems are constructed by solving the laws governing the conservation of mass, momentum, and energy for each phase individually with the interfacial conditions. These analyses require reliable data on heat and mass transfer coefficients during the regeneration processes. This has been proved to be difficult and most researchers have used simplified analytical models with sound simplifying assumptions to reduce the computational effort [13-16].

Artificial neural network (ANN) models have become very popular recently to overcome some of the limitations of physical modeling. ANN models are capable of relating output to input variables for cases where no theoretical model works satisfactorily in a realistic time frame. An artificial neural network is an information-processing paradigm inspired by the manner in which the heavily interconnected parallel structure of the human brain processes information [17-19]. They are collections of mathematical processing units that emulate some of the observed properties of biological nervous systems and draw on the analogies of adaptive biological learning. ANN models are trainable systems whose learning abilities, generalization capabilities, and tolerance to uncertainty and noise are derived from their distributed network structure and knowledge representation [19].

The present work proposes the use of an ANN based model in order to capture the correlations between inlet parameters and

* Corresponding author. Tel.: +966530548066
Fax: +96627255529; E-mail: ezeidan2002@yahoo.com

DOI: 10.5383/ijtee.01.02.005

the performance of the solar-powered packed-bed desiccant regenerator. These correlations would satisfy the basic laws of conservation of mass, momentum, and energy. Outlet values for different inlet states available from experimental data are used to construct and validate the ANN model. It is also objected to evaluate the regenerator effectiveness as well as the overall value of the system coefficient of performance (COP) in a typical solar-powered condition.

2. Packed-Bed Model

2.1. Basic definitions

To model the dehumidification/regeneration column, consider the counter current air-desiccant liquid-column (assumed to be calcium chloride ($CaCl_2$) solution) shown in Fig. 1. The cross section of the tower is *S*, and the height of the contact section is dz. Air at humidity ratio, $\omega_{a,i}$, and temperature, $T_{a,i}$, enters the bottom of the column and leaves at the top with humidity ratio $\omega_{a,o}$ and temperature $T_{a,o}$. Liquid enters the top at temperature $T_{L,i}$ and leaves from the bottom at temperature $T_{L,o}$. The mass velocity of air is G_a, the mass of vapor free gas per unit area of tower cross section per second. The mass velocities of the liquid at the inlet and outlet are $G_{L,i}$ and $G_{L,o}$, respectively. Let dz be the height of a small element of the tower at distance *z* from the bottom of the column. The mass velocity of the liquid at the height *z* is G_L, the temperature of gas and liquid are T_a and T_L, respectively, and the humidity ratio is ω. At the interface between the gas and liquid phases, let the temperature be T_i and the humidity ratio be ω_i.

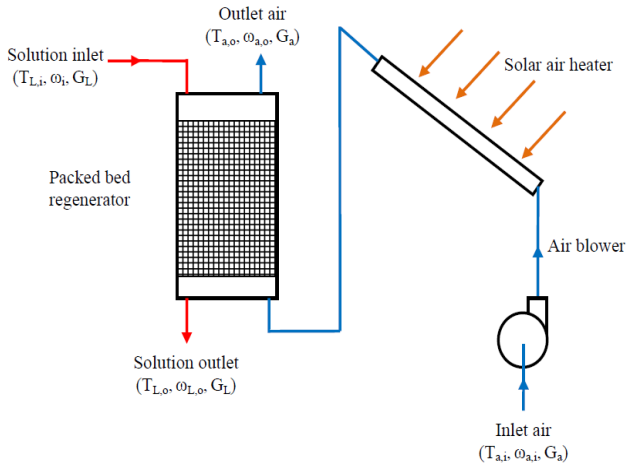

Fig. 1. Schematic of packed-bed solar-powered regenerator

2.2. Heat and mass balance for the air and liquid sides

Considering the small volume Sdz, the mass and heat balances for the air and liquid desiccant sides can be written as follows [20]:

The enthalpy balance is:

$$G_a dH_a = G_L dH_L \tag{1}$$

where H_a and H_L are the specific enthalpies of the air and liquid desiccant solution, respectively. The rate of heat transfer from the air to the interface is:

$$G_a C_a dT_a = h_a (T_a - T_i) a_H dz \tag{2}$$

where C_a is the air specific heat, h_a is the heat transfer coefficient from the air to the interface and a_H is the heat transfer area per unit contact volume. The rate of the mass transfer of the vapor from the interface to the gas is:

$$G_a d\omega = K_a (\rho_i - \rho) a_M dz \tag{3}$$

where K_a is the mass transfer coefficient, ρ_i, ρ are the vapor density in the interface and in the flowing air at the small volume Sdz. a_M is the mass transfer area per unit contact volume.

The rate of heat transfer from the interface to the liquid is:

$$G_L dH_L = h_L (T_i - T_L) a_H dz \tag{4}$$

If the liquid flow rate is assumed to be constant with height, then:

$$G_L dH_L = G_L C_L dT_L \tag{5}$$

Substituting from Eq. (5) into Eq. (4) gives:

$$G_L C_L dT_L = h_L (T_i - T_L) a_H dz \tag{6}$$

where C_L is the specific heat of the liquid desiccant solution.

2.3. Rate of water evaporation

The rate of water evaporation from the desiccant solution is the main parameter which determines the cooling effect of the desiccant cooling system. Integrating Eq. (3), we can get the rate of water evaporation as:

$$m = \int G_a d\omega = \int K_a (\rho_i - \rho) a_M dz \tag{7}$$

In the above equation, the potential for mass transfer from the interface to the air side is the difference in vapor density, which can be evaluated in terms of vapor pressure. However, the vapor pressure on the desiccant solution surface can be evaluated by knowledge of the solution temperature and concentration [21-23].

2.4. Regeneration column performance

The performance of a regeneration column can be evaluated by a specific column effectiveness which is defined as the ratio between the absolute value of the actual humidity change on the air side and the absolute value of the maximum humidity change possible under given conditions. In case of regeneration, the regenerator effectiveness, ε, is the ratio of the actual change in humidity ratio of the air passing through the regenerator to its variation under ideal conditions, as

$$\varepsilon = \frac{\omega_{a,o} - \omega_{a,i}}{\omega_{e,\max} - \omega_{a,i}} \tag{8}$$

where $\omega_{e,\max}$ is the specific humidity of air at equilibrium with solution having maximum value of vapor pressure. The maximum value of vapor pressure on the solution surface depends on its temperature and concentration.

2.5. System coefficient of performance

The overall coefficient of performance of the system can be evaluated from the following expression:

$$COP = \frac{Q}{IA_c} \tag{9}$$

where I is the solar radiation intensity in the collector surface, A_c is the collector area and Q is the cooling rate of the desiccant cooling system, which can be evaluated by multiplying the rate of water evaporation m by the latent heat of water L at the evaporator pressure i.e.,

$$Q = m(LH)_{ev} \tag{10}$$

The regeneration heat, Q_g, in case of solar air heater can be evaluated from the following

$$Q_g = IA_c\eta_c \tag{11}$$

where η_c is the collector efficiency. For solar air heaters, the collector efficiency is dependent on the collector design parameters and the ambient conditions [24]. A common expression used for evaluating the air heater efficiency is given as:

$$\eta_c = A - B\frac{T_{c,i} - T_{amb}}{I} \tag{12}$$

where A, B are constants, dependent on the design conditions [25].

The above mentioned analysis shows the dependence of the regeneration process on operational parameters such as air and liquid mass flow rates as well as temperature of the hot air. In this study, a trained neural network model based on the back-propagation algorithm is used for the system performance analysis.

3. Neural network (ANN) model

3.1. ANN model structure

Fig. 2 shows the architecture of the neural network model used in this work. The basic structure is a multilayer ANN model where the chosen six inputs are fed into the first layer of hidden units. There, the circles represent the neurons (weights, bias, and activation functions) and the lines represent the connections between the inputs and neurons, and between the neurons in one layer and those in the next layer. Several studies have found that a three-layered neural network, where there are three stages of neural processing between the inputs and outputs, can approximate any nonlinear function to any desired accuracy [19].

Each layer consists of units which receive their input from units from a layer directly below and send their output to units in a layer directly above the unit. Each connection to a neuron has an adjustable weighting factor associated with it. The output of the hidden units is distributed over the next layer of hidden units, until the last layer of hidden units, of which the outputs are fed into a layer of no output units. Training of the ANN model typically implies adjustments of connection weights and biases so that the differences between ANN outputs and desired outputs are minimized.

3.2. Back-propagation training algorithm

Back-propagation training, used in this investigation, is one of the most popular ANN training methods. The basic back-propagation algorithm adjusts the weights in the steepest descent direction (negative of the gradient). This is the direction in which the error decreases most rapidly. To explain the back-propagation rule in detail, the three-layer network shown in Fig. 2 will be used. The training phase is divided into two phases as follows:

1. <u>*Forward-propagation phase:*</u> In the first phase, input data are sent from the input layer to the output layer, i.e., X=[X_1:X_6] is propagating from the input layer to the output layer Y=[Y_1:Y_4].

$$Z_q = f\left(\sum_j V_{qj}X_j\right) \tag{13}$$

$$Y_i = f\left(\sum_q W_{iq}Z_q\right) \tag{14}$$

where W_{iq} and V_{qj} represent weights in the hidden-to-output and input-to-hidden connections, respectively.

2. <u>*Back-propagation phase*</u>: In the second phase, the errors between target outputs, *y*, and predicted outputs, *d*, are calculated and propagated backwardly to the input layer in order to change the weights of hidden layers by using the gradient descent method.

The algorithm tries to minimize the objective function, i.e. the least square error between the predicted and the target outputs, which is given by:

$$E = \frac{1}{2}\sum_p (d_o{}^p - y_o{}^p)^2 \tag{15}$$

where p represents the number of training datasets and o represents the number of output nodes. Then the algorithm uses the steepest-descent direction to adjust the weights in the hidden-to-output and input-to-hidden connections and as follows:

$$\Delta W_{iq} = -\lambda\frac{\partial E}{\partial W_{iq}}, \Delta V_{qji} = -\lambda\frac{\partial E}{\partial V_{qj}} \tag{16}$$

where λ is (3).

Since this algorithm requires a learning rate parameter to determine the extent to which the weights change during iteration, i.e., the step sizes, its performance depends on the choice of the value of the learning rate. The two phases are iterated until the performance error decreased to certain small range [19].

(a)

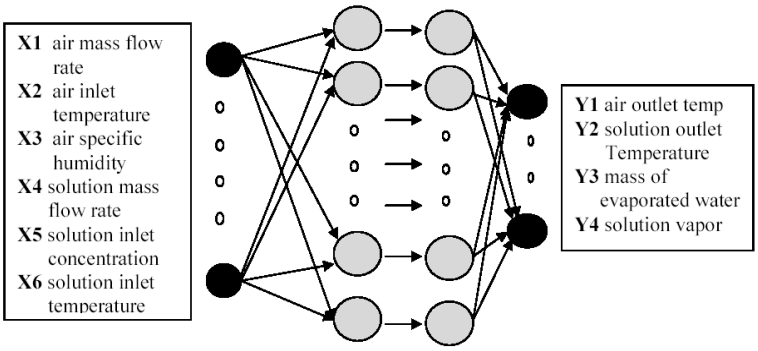

(b)

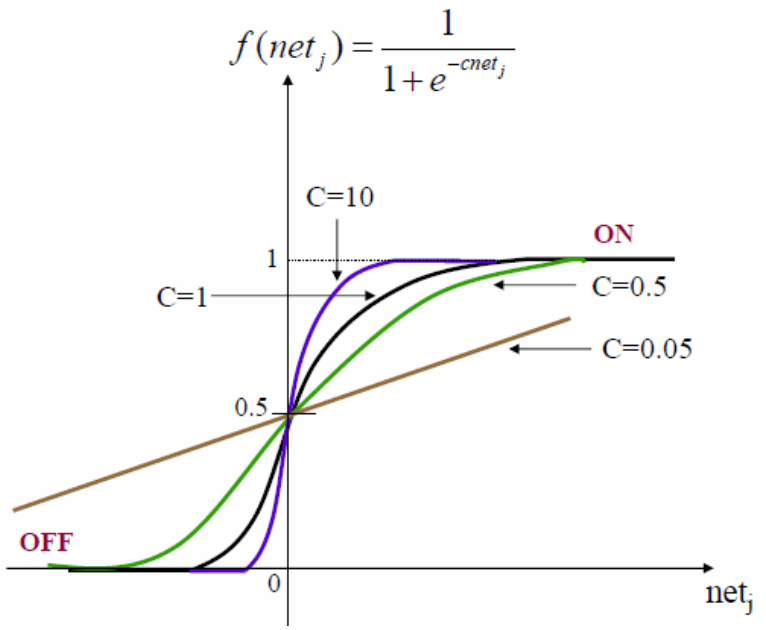

Fig. 2. (a) A schematic of neural network model. (b) The sigmoid activation function with different values of C

3.3. Activation functions

Activation functions are used in ANNs to produce continuous values rather than discrete ones. The activation functions used in hidden layer neurons are tan sigmoid functions and the piecewise linear activation function is used for the last layer neurons. The logistic activation function or more popularly referred to as the sigmoid function is semi-linear in character, differentiable and produces a value between 0 and 1. The mathematical expression of this sigmoid function is:

$$f(net_j) = \frac{1}{1+e^{-c(net_j)}} \qquad (17)$$

where c controls the firing angle of the sigmoid. When c is large, the sigmoid becomes like a threshold function and when is c small, the sigmoid becomes more like a straight line (linear). When c is large learning is much faster but a lot of information is lost, however when c is small, learning is very slow but information is retained. Because this function is differentiable, it enables the back-propagation algorithm to adapt the lower layers of weights in a multilayer neural network. All the six input variables and their range of values used to develop the neural network model are listed in Table 1. The output variables and the tolerances for training, validation, and testing data sets are listed in Table 2.

4. Results and discussion

The air and solution outlet parameters have been estimated using the neural network model and compared with experimental measurements of Sultan et al. [8]. The developed model was validated by comparing the model output and the actual data obtained from the experiments. Table 2 shows the relative percentage error in training and validation of the output variables. The results show that the errors are below 1% for most of the variables. The maximum error is about 3.5% in the values of the mass of evaporated water. This can be explained by the fact that the experimental value of the mass of evaporated water is actually evaluated from the measured values of the solution concentration (vapor pressure and temperature). Therefore, the error in the evaluated value of water evaporation rate is expected to be higher than that for the temperature and vapor pressure. It can be concluded that the neural network model provides correct values for all the output variables which is evidenced by good agreement between the outputs from the model and the corresponding experimental measurements.

Fig. 3 shows a comparison between the trained data of the ANN model and the experimental data for all the output variables with respect to the air inlet temperature. Good agreement is found between the trained data of the model and the experimental measurements for the whole range of the air inlet temperature. Similarly, good agreement can be shown in Fig. 4 in the comparison between the trained data of the ANN model and the experimental data for all the output variables with respect to the air mass flow rate.

Then the model is applied to test the performance characteristics of the system under the specified conditions. One of the important performance parameters is the regenerator effectiveness which is defined by actual change in air humidity ratio to the maximum possible change (Eq. (8)) is plotted versus air mass flow rate as shown in Fig. 5. It can be observed that, for the specified operating conditions of the packed bed, the effectiveness gradually increases with the solution flow rate. This can be explained by the fact that: as air is the heating medium, successive increase in air flow rate results in higher values of the vapor pressure on the solution surface and consequently higher potential for mass transfer from desiccant to air. The same result is expected also when the temperature of the heating medium (air in the preset study) increases. Fig. 6 demonstrates the effect of air inlet temperature on the regenerator effectiveness. The effectiveness increases gradually with the increase of the air inlet temperature due to the fact (5)

When solar air heater is applied to power the desiccant regenerator, a moderate operating condition is assumed to assess the system performance. The solar air heater is selected as given in [8] and the collector efficiency is evaluated from Eq. (12) and the constants A and B are considered as follows: A=0.7273 and B=14.9. Figure 7 shows the effect of air temperature on the COP of the desiccant cycle as well as the system. It is clear that the value of COP decreases with increase in air temperature. However, the range of air temperature in this analysis is selected taking into account the limitations of the solar collector performance when air is heated rather than liquid. It can be also noted that as the air temperature increases from 52 to 60 ^{o}C, the decrease in cycle performance is not sound as that for the system. This can be explained by the effect of air temperature on the collector efficiency, which is linearly decreasing with increase in air temperature.

5. Conclusion

The performance of a solar-powered desiccnt regenerator has been investigated using an artificial neural network (ANN) approach. The neural network model is implemented and its feasibility is established. In addition to its simplicity, the proposed methodology results in some desirable characteristics including its wide range of application. Good agreement between the outputs from the ANN model and the corresponding results from the experimental measurements are found. It is also concluded that the proposed model can be successfully used for predicting the overall performance of the system on the basis of experimental data collected for different system parts from the litrature.

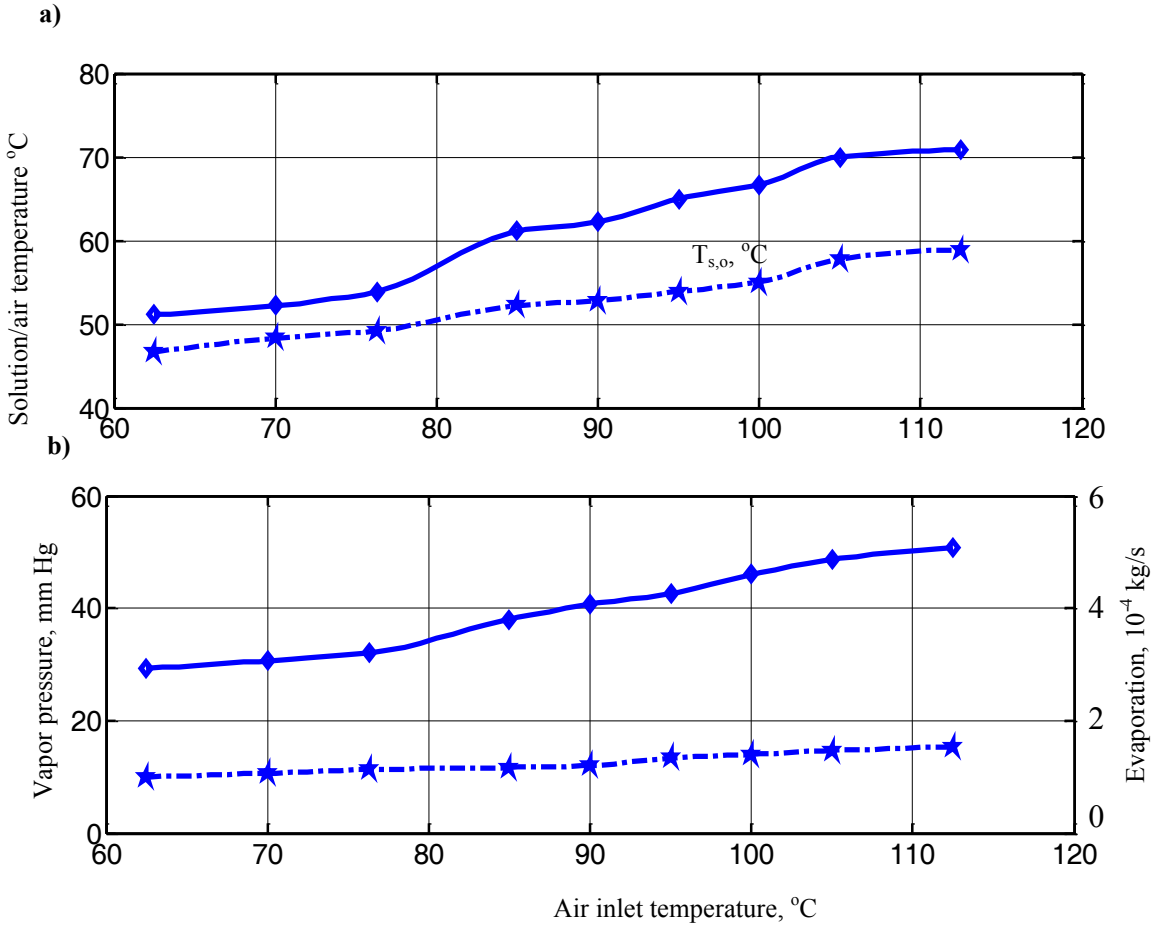

Fig. 3. Comparison between the trained data of the ANN model and experimental measurements (effect of air inlet temperature). a) Solution and air temperatures. b) Vapor pressure on the solution surface and mass of evaporated water

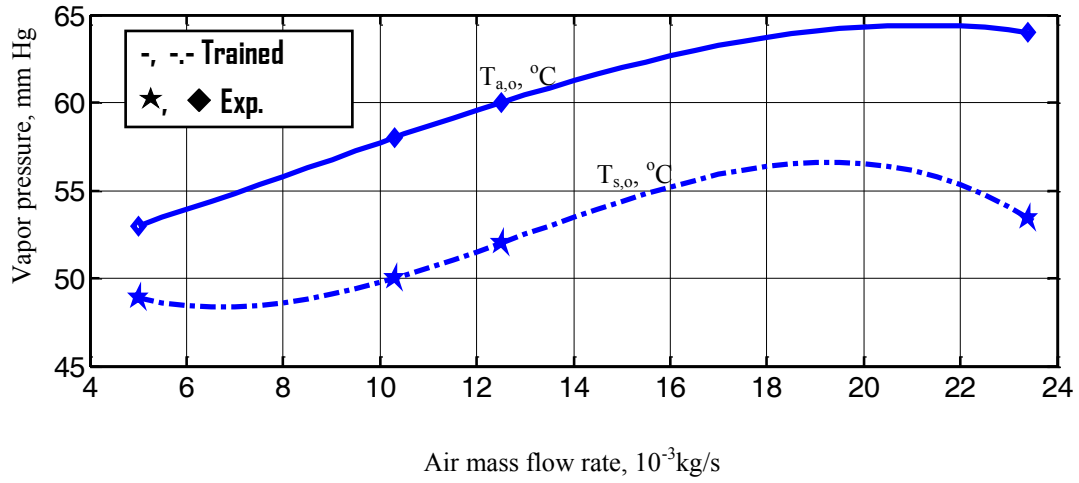

Fig. 4. Comparison between the trained data of the ANN model and experimental measurements (effect of air mass flow rate)

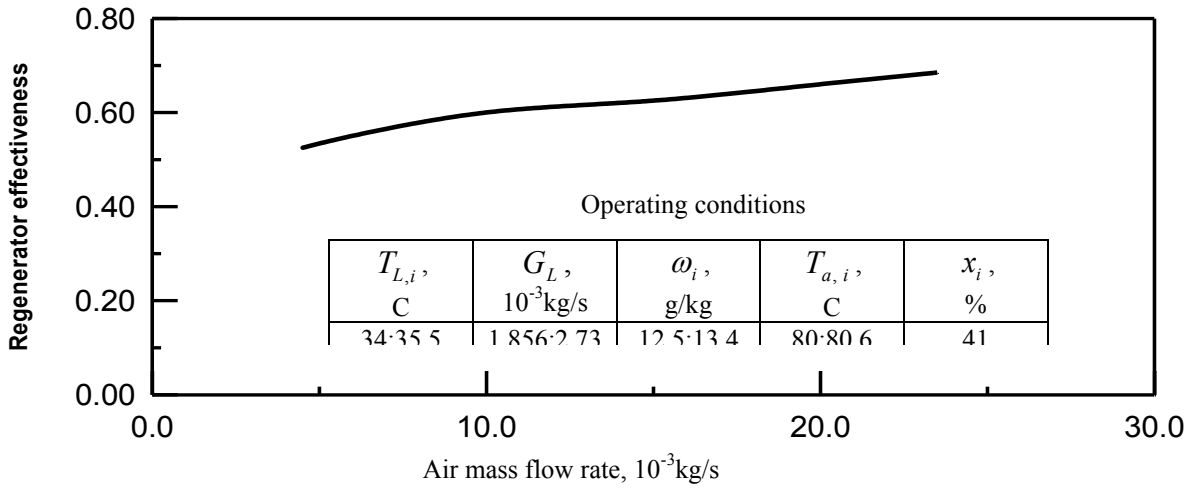

Fig. 5. Effect of air mass flow rate on the regenerator effectiveness

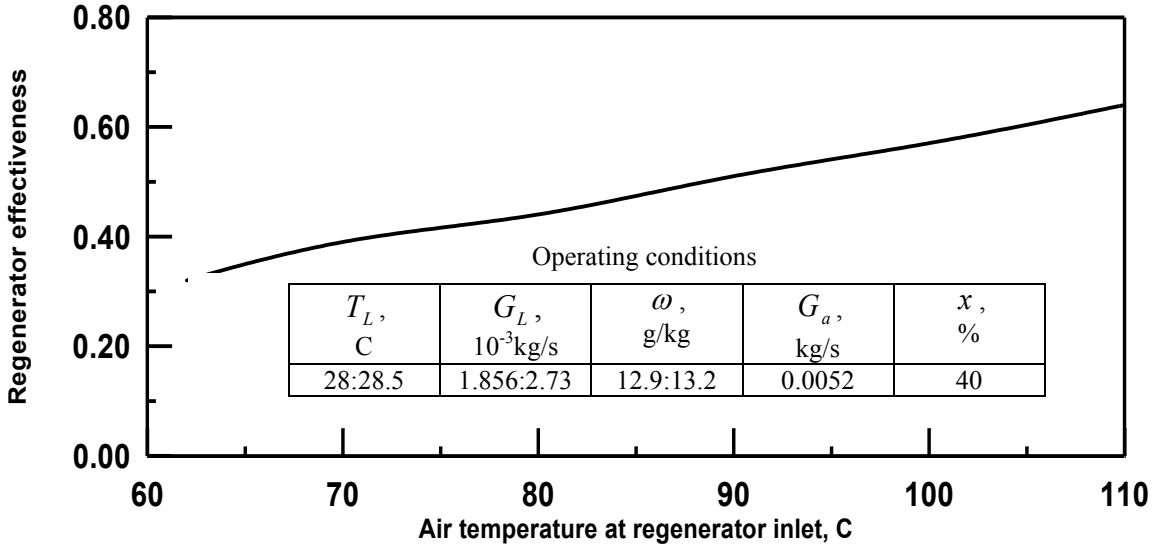

Fig. 6. Effect of regeneration temperature on the regenerator effectiveness

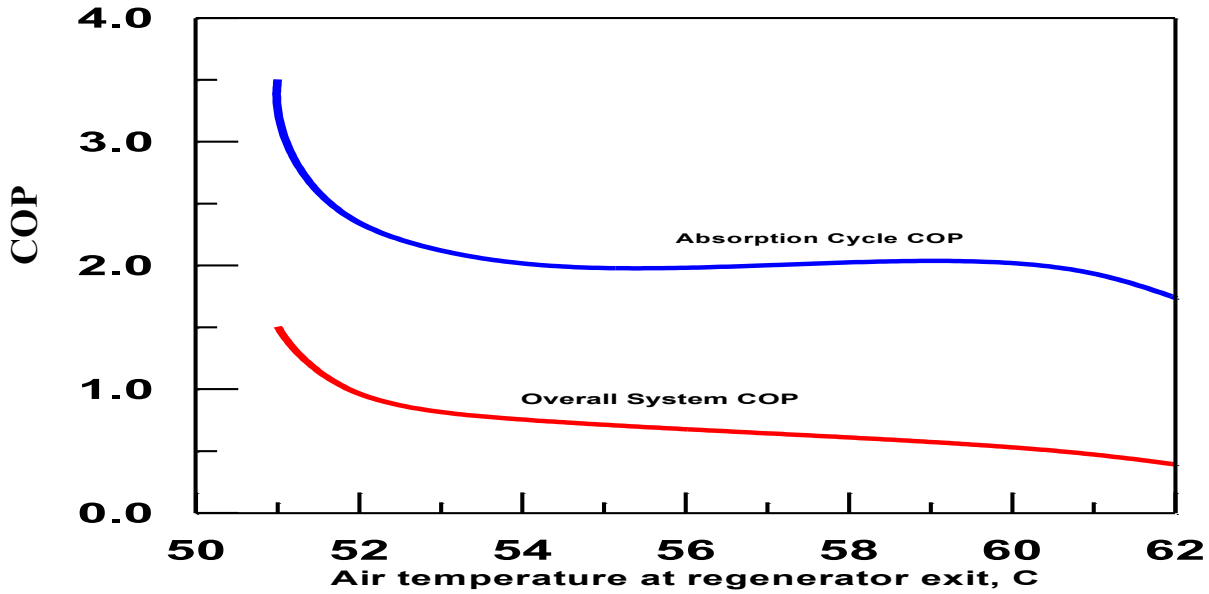

Fig. 7. Effect of air temperature at regenerator exit on the coefficient of performance

Nomenclature

A	constant in Eq. (12)
A_c	collector surface area, m^2
a	transfer area, m^2/m^3
B	constant in Eq. (12)
C	specific heat, $J/kg\ K$
d	target output for ANN model
E	sum square error
H	specific enthalpy, J/kg
h	heat transfer coefficient, $W/m^2\ °C$
I	solar radiation intensity, W/m^2
G	fluid mass velocity, $kg/m^2\ s$
K_a	mass transfer coefficient, m/s
LH_{ev}	latent heat of evaporation, J/kg
m	rate of water evaporation, kg/s
Q	cooling heat rate, W
Q_g	regeneration heat rate, W
S	cross section area, m^2
T	temperature, $°C$
V	weight factors in the input-to-hidden connections
W	weight factors in the hidden-to-output connections
X	input set for ANN model
Y	output set for ANN model
Z	data set for hidden layers
z	bed height, m

Greek Symbols

ε	effectiveness
η	collector efficiency
λ	rate of learning
ρ	density, kg/m^3
ω	air specific humidity, kg_w / kg_a

Subscripts

a	air
amb	ambient
c	collector
e	equilibrium
i	inlet
i, j, q	indices
L	liquid
o	outlet
max	maximum

Acknowledgements

The authors would like to acknowledge the financial support of the University of Taif, Saudi Arabia.

References

[1] Daou K, Wang RZ, and Xia ZZ. Desiccant cooling air conditioning: a review. Renewable and Sustainable Energy Reviews 2006 ; 10 : 55–77. http.dx.doi.org/10.1016/j.rser.2004.09.010

[2] Smith RR, Hwang CC, and Dougall RS. Modeling of a solar-assisted air conditioner for a residential building. Energy1994; 19 (6): 679-91. http.dx.doi.org/10.1016/0360-5442(94)90007-8

[3] Grossman G. Solar-powered systems for cooling, dehumidification and air-conditioning. Solar Energy 2002;72:53–62. http.dx.doi.org/10.1016/S0038-092X(01)00090-1

[4] Gandhidasan P, and Al-Farayedh AA. Solar regeneration of liquid desiccants suitable for humid climates. Energy 1994;19(8):831-6. http.dx.doi.org/10.1016/0360-5442(94)90035-3

[5] Dieckmann J, Roth K, and Brodrick J. Liquid Desiccant Air Conditioners. ASHRAE Journal, Oct. 2008;90-95.

[6] Best R, and Ortega N. Solar refrigeration and cooling. Renewable Energy 1999;16:685-690. http.dx.doi.org/10.1016/S0960-1481(98)00252-3

[7] Martin V, and Goswami DY. Effectiveness of heat and mass transfer processes in a packed bed liquid desiccant dehumidifier/regenerator. HVAC&R Research *2000;*6:21–39.

[8] Sultan GI, Hamed AM, and Sultan AA. The effect of inlet parameters on the performance of packed tower regenerator. Renewable Energy 2002;26:271–283. http.dx.doi.org/10.1016/S0960-1481(01)00113-6

[9] Liu XH, Jiang Y, Chang XM, and Yi XQ. Experimental investigation of the heat and mass transfer between air and liquid desiccant in a cross-flow regenerator. Renewable Energy 2007; 32: 1623–1636. http.dx.doi.org/10.1016/j.renene.2006.07.002

[10] Jain S, Dhar PL, and Kaushik SC. Experimental studies on the dehumidifier and regenerator of a liquid desiccant cooling system. Applied Thermal Engineering 2000;20(3):253–67. http.dx.doi.org/10.1016/S1359-4311(99)00030-7

[11] Abdul-Wahab SA, Zurigat YH, and Abu-Arabi MK. Predictions of moisture removal rate and dehumidification effectiveness for structured liquid desiccant air dehumidifier. Energy 2004; 29 (11): 19-34. http.dx.doi.org/10.1016/j.energy.2003.08.001

[12] Gommed K, and Grossman G. Experimental investigation of a liquid desiccant system for solar cooling and dehumidification. Solar Energy 2007;81:131-138. http.dx.doi.org/10.1016/j.solener.2006.05.006

[13] Babakhani D, and Soleymani M. An analytical solution for air dehumidification by liquid desiccant in a packed column. International Communications in Heat and Mass Transfer 2009; 36: 969-977. http.dx.doi.org/10.1016/j.icheatmasstransfer.2009.06.002

[14] Longo GA, and Gasparella A. Experimental and theoretical analysis of heat and mass transfer in a packed column dehumidifier/regenerator with liquid desiccant. The International Journal of Heat and Mass Transfer 2005;48:5240-5254. http.dx.doi.org/10.1016/j.ijheatmasstransfer.2005.07.011

[15] Hamed AM. Theoretical and experimental study on the transient adsorption characteristics of a vertical packedporous bed. Renewable Energy 2002;27:525-541. http.dx.doi.org/10.1016/S0960-1481(01)00112-4

[16] Khan AY, and Ball HD. Development of a generalized model for performance evaluation of packed-type liquid sorbent dehumidifiers and regenerators. ASHRAE Transactions 1992;98:525–533.

[17] Virk GS, and Al-Dmour A. System Simulation Using Neural Networks. Departmental Research Report no. 537, University of Bradford; Jan. 1994.

[18] Jantzen J. Neurofuzzy Modelling. Lyngby Tech Report no. 98-H-874, Denmark; Oct. 1998.

[19] Aly AA. Flow rate control of variable displacement piston pump with pressure compensation using neural network. Journal of Engineering Science 2007;33(1):199-209.

[20] McCabe WL, Smith JC, and Harriott P. Unit operation of chemical engineering. McGraw-Hill; 1985.

[21] Zaetsev ED, and Aseev GG. Physical–chemicalproperties of binary non-organic solutions. Khemia; 1988.

[22] Hamed AM. Absorption–regeneration cycle for production of water from air-theoretical approach. Renew Energy Journal 2000;19:625–635. http.dx.doi.org/10.1016/S0960-1481(99)00068-3

[23] Gandhidasan P, Mohandes MA. Predictions of vapor pressures of aqueous desiccants for cooling applications by using artificial neural networks. Applied Thermal Engineering 2008;28:126–135. http.dx.doi.org/10.1016/j.applthermaleng.2007.03.034

[24] Chudhury C, and Garg HP. Design analysis of corrugated and flat plate solar air heaters. Renewable Energy 1991; 1 (5/6): 595-607. http.dx.doi.org/10.1016/0960-1481(91)90003-8

[25] Ozgen F, Esen M, and Esen H. Experimental investigation of thermal performance of a double-flow solar air heater having aluminum cans. Renewable Energy 2009; 34: 2391–2398. http.dx.doi.org/10.1016/j.renene.2009.03.029